Construction and Building Materials 467 (2025) 140376

Contents lists available at ScienceDirect

Construction and Building Materials

journal homepage: www.elsevier.com/locate/conbuildmat

Modeling an artificial neural network to estimate cement consumption in clayey waste-cement mixtures based on curing temperature, mechanical strength, and resilient modulus

Liliana Carolina Hernández García [a,1], Julián Vidal Valencia [b,2], Henry A. Colorado L [a,*,3]

[a] CCComposities Laboratory, Universidad de Antioquia UdeA, Calle 70 No. 52-21, Medellín 050010, Colombia
[b] Engineering Materials Research Group (GME), Universidad Eafit, Medellín, Carrera 49 N° 7 Sur-50, Medellín, Colombia

ARTICLE INFO

Keywords:
Artificial network
Artificial Intelligence
Soil cement
Clay waste
Resilient modulus
Clay soil
Waste

ABSTRACT

Seeking to address large-scale issues faced by many countries today, such as excessive energy consumption, global warming, and uncontrolled mining activities, this research repurposes clayey mining and excavation waste to design soil-cement mixtures for road construction. A total of 2026 data points from laboratory experimental tests were statistically analyzed using regression models and neural networks to evaluate the effect of curing temperature on compressive strength, indirect tensile strength, and resilient modulus. The study focused on three types of clayey waste mixed with high early-strength hydraulic cement (Type 1 Portland cement) after 7 days of curing. The samples were cured in three different chambers, each maintaining a constant temperature of 10, 28, and 40 °C for 7 days, simulating the most common road temperatures in Colombia. Results showed that temperature has a positive effect of 18 % on the resilient modulus, which could lead to cement savings in warm climates. Additionally, an artificial neural network model was developed, which can contribute to the construction and design of more sustainable and environmentally friendly geothermal pavements. The use of these models and networks not only facilitates the study of multiple variables but also optimizes materials and methods, aiming to reduce energy consumption and costs.

1. Introduction

The Sustainable Development Goals 2023 Report highlights new challenges in terms of infrastructure [1]. In 2022, only 51.6 % of the world's urban population had access to public transport. Particularly in developed countries, people have more than one transportation option, while in the poorest developed countries people lack access to roads despite increasing demand for mobility. On the other hand, global consumption of raw materials has increased by 66 % since the 1970s, resulting in a per capita material footprint of 95.9 billion metric tons.

To ensure the efficiency and competitiveness of the transport sector, greener construction materials are being evaluated. These materials reduce the exploitation of virgin aggregates by using construction and demolition waste or recycled materials instead [2,3]. The performance and durability of pavement structures depend on the quality of the subgrade. For this reason, publications focus on the characterization of pavement materials, subgrade, granular layers, and asphalt mixtures through repeated triaxial load testing [4].

For this reason, research on soil resilience have significantly increased over the last 10 years. The publications aimed at establishing mathematical models for predicting resilient modulus pavements have grown exponentially. As shown in Fig. 1, the last 10 years 3806 publications research on resilient soil modulus, 607 focus on resilient module pavements, and eighty-seven address resilient modulus prediction models for subgrades, for a total of 4500 documents in 10 years.

From these documents, 75 % are research articles, 10 % are review articles, 10 % are book chapters, 2 % are part of encyclopedias, 2 % are short communications, and the remaining 1 % are papers, see Fig. 2. These statistical data align with reports from the United Nations, which clearly outline the needs regarding the exploitation of non-renewable

* Corresponding author.
E-mail address: henry.colorado@udea.edu.co (H.A. Colorado L).
[1] https://orcid.org/0000-0003-2735-5621
[2] http://orcid.org/0000-0002-3519-2052
[3] http://orcid.org/0000-0003-4948-0482

https://doi.org/10.1016/j.conbuildmat.2025.140376
Received 15 October 2024; Received in revised form 3 February 2025; Accepted 7 February 2025
Available online 12 February 2025

resources, mobility, and resilient infrastructures. Combined with innovative technologies, the use of artificial intelligence and neural networks has led to increased interest within the scientific community in designing and testing resilient materials that ensure the quality and durability of infrastructure.

From this bibliographic search, publications containing databases with results from resilient modulus tests were selected. The minimum, maximum, and mean Resilient Modulus (RM) will be determined as comparison parameters. The calculation method and the number of recorded data were filtered. Materials mixed with asphalt binder, RAP, or granular materials were removed, leaving only the resilient modulus values of subgrade soils, as shown in Table 1.

Cluster analysis using R Studio results in a three-group classification, as shown in Fig. 3. The recorded resilient modules are related to the amount of data and the calculation method, using the Hubert index and the D index, which are graphical methods to determine the number of clusters, measured at the inflection point [33].

Group 3 is the most distinct, with databases that are similar within the group. Its range is quite wide, with the lowest modulus at 3 MPa and the highest at 360 MPa, and an average of 34 MPa. Meanwhile, Groups 1 and 2 consist of improved soil tests where the variability of the data is due to changes in moisture and confining pressure. The average modulus for Group 1 is 100 MPa, while the average modulus for Group 2 is 223.2 MPa.

Studies show that the variables that most influence the calculation of the Resilient Modulus are the type of soil, the content of stabilizing materials such as cement, lime, and fly ash, as well as the soil's plasticity index, moisture content, and silt content [34]. However, when vehicular loads pass through, pavement materials are exposed to cyclic compressive stresses (σ_c) and tensile stresses (σ_t) that induce deformations, which tend to accumulate depending on the initial stiffness of the materials. In fact, cracks and deformations can appear at stress levels much lower than the material's strength [35].

For this reason, pavement design methods establish sufficient thicknesses to prevent not only excessive permanent deformation but also surface cracking. Based on elastic theory for layered systems, it is possible to predict the transient deformations of a pavement [36]. Fatigue failures result from instantaneous processes as well as plastic or permanent deformations, which can be measured through cyclic laboratory tests.

However, it is important to consider that prediction models are affected by material characteristics such as thixotropy, also known as the initial loading age. This property was identified by Seed, Chan, and Lee (1964) after measuring the resilience in failed samples of different ages. The initial resilient stress increases as the time interval between compaction and testing increases. In the experimental validation by Seed, Chan, and Lee, the sample with the greatest age recorded moduli five times higher than those of the samples tested after only 15 min. However, after 500 cycles, the resilient modulus curves converged at a single point, indicating that the effect of thixotropy had dissipated [37].

Thixotropy is a phenomenon inherent to remolded soils and is based on the recovery of strength when the soil is at rest again. In other words, the initial resilience records are apparent high values that decrease after the application of several loading cycles, as the soil recovers its shape memory and initial stress state. Testing standards recommend applying between 500 and 1000 loading cycles to condition the sample and thus avoid the effects of thixotropy in the result [38].

Other factors that influence the resilience of fine granular soils include the number of load applications, chamber pressure, compaction method, sample density, and moisture content at the time of testing [39]. On the other hand, the factors that affect the resilience of coarse granular soils include the nature of the rock, solidity index, maximum particle size, angularity, roughness, and gradation [40].

Testing standards establish different magnitudes for chamber pressure, axial stress, and cyclic stresses to measure the resilient modulus in fine soils and coarse soils. Likewise, the resilient modulus and deviatoric stress diagrams are expected to show different trends, as illustrated in Fig. 4(a) where a resilient modulus diagram for a clay and Fig. 4(b) a diagram for a granular base are shown. Usually, fine granular soils record high moduli at low deviatoric stress, but as this stress increases, the moduli decrease, converging at a single point.

Fig. 4(a) shows the results of a resilient modulus test where the modulus starts at 58 Mpa, but after 60 kPa it is reduced to 45 Mpa. The three confining pressures converge at higher deviatoric stress. In contrast, coarse granular soils exhibit an opposite behavior, where the resilient modulus increases as the deviatoric stress increases, showing an

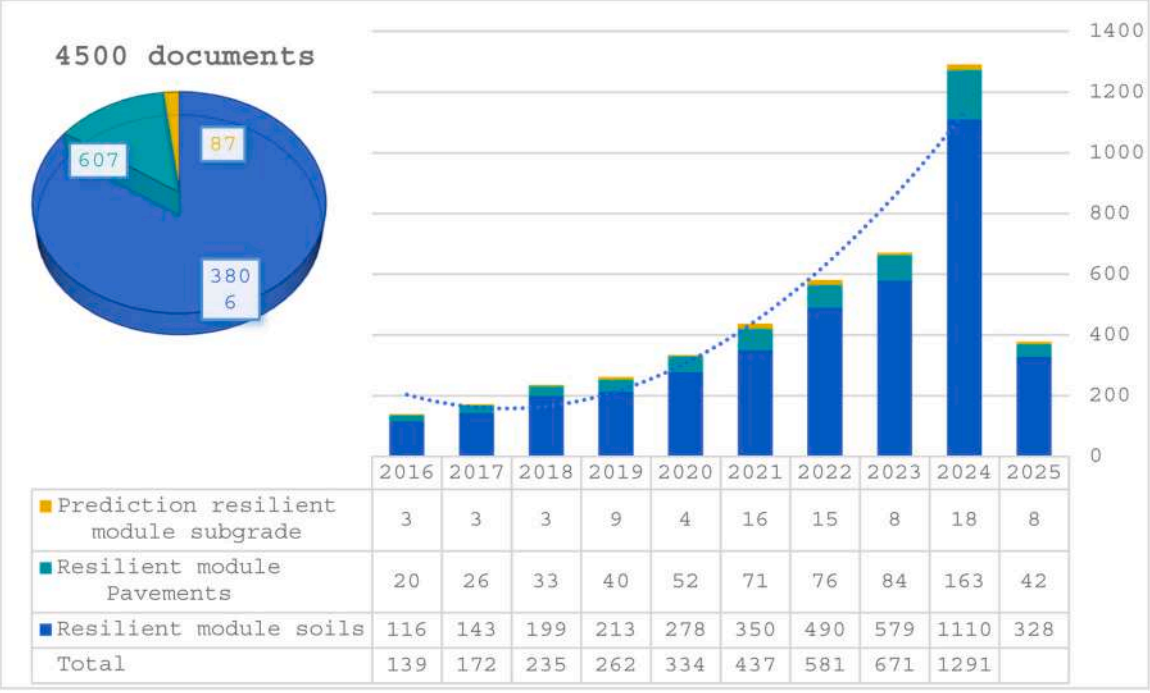

	2016	2017	2018	2019	2020	2021	2022	2023	2024	2025
Prediction resilient module subgrade	3	3	3	9	4	16	15	8	18	8
Resilient module Pavements	20	26	33	40	52	71	76	84	163	42
Resilient module soils	116	143	199	213	278	350	490	579	1110	328
Total	139	172	235	262	334	437	581	671	1291	

Fig. 1. Number of publications per year since 2016 taken from the database ScienceDirect.

upward trend. Fig. 4(b) shows that with a deviatoric stress of 30 it is relatively low compared to a modulus measured with a stress of 150 kPa. Thus, indicating that the greater the confinement and the greater the deviatoric stress, the greater the resilient modulus.

Based on these trends, various methods for calculating and predicting resilient moduli have been developed, as summarized in Table 2.

The variables analyzed in the models are: $\sigma 2 = \sigma 3 = \sigma c =$ confining pressure, $\theta =$ bulk normal stress, $\sigma di =$ deviator stress at which the slope of the MR versus σd changes. K1, k2, k3, K6, and K7 are regression parameters ($k1 \geq 0$, $k2 \geq 0$, $K6 \leq 0$ and $K7 \geq 1$), Pa = atmospheric pressure, $\tau oct =$ octahedral shear stress, $\tau_{ref} =$ reference shear stress, $Wc_{opt} =$ optimum water content, Wc = a certain water content, c = cohesion, $\varnothing =$ internal friction angle in degree, UC = unconfined strength, MC = moisture content, Ki, ai, Ai, ci, $\alpha 1$, $\alpha 2$, $\beta 1$, m = fitting parameters. $u_m =$ matric soil suction in kPa. α, γ, β, and φ are the fitting parameters, θr is the reduced normal stress at reference water content in MPa, and τr is the reduced octahedral shear stress at reference water content in MPa.

Despite advances in predicting the resilient modulus, there are limited publications that address the effect of curing temperature. Heat transfer in materials, as well as behavior under thermal loads, are important parameters in the design of geothermal pavements. The performance of geothermal pavements is affected by ambient temperature, the effects of the urban heat island (UHI) [56], location, and the materials used [57]. However, studies indicate that a thermal performance of 50 watts per square meter of geothermal pavement can be achieved. With an optimal design, this can meet the heating and cooling demands of nearby buildings [58].

On the other hand, pavements are structures with most of their surface exposed to weather conditions. For this reason, their mechanical behavior and costs largely depend on ambient temperature [59,60]. The effect of a positive temperature gradient (which occurs during the day) tends to deform hydraulic concrete pavements into a concave shape, while a negative temperature gradient (which occurs during the night) deforms pavements into a convex shape. It is known that higher elasticity, greater thermal expansion coefficient, and lower thermal conductivity can lead to greater curvature stresses and movement in concrete pavements [61].

For this reason, and unlike previously published research, this study aims to provide a neural network model that not only includes traditionally validated variables but also incorporates others such as thermal conductivity, curing temperature, and organic matter content. The goal is to serve as a design parameter and quality control tool in the construction of geothermal pavements, using excavation waste with varying organic matter content installed in different climates.

2. Material and methods

The experimental design was based on a full factorial 3k design, with 2 factors, each with three level, see Table 3. Three types of soils were used, with different plasticity indices (PI: 0; 35 %; 66 %) cured at three different temperatures (T = 10; 28; 40°C), simulating the most common climates in the regions of Colombia. In this way, the 3k model is completed, with a minimum value, a maximum value, and an average value of each variable to analyze. A total of 2026 resilient modulus replicates were performed, following the T307–99 AASHTO test methodology. From the same mixture, the dry density, thermal conductivity, compressive strength, indirect tensile strength, plasticity index, methylene blue value, and organic matter content by loss on ignition were measured.

2.1. Soil

Each soil corresponds to pulverized waste from demolition and construction activities. Soil 01 is the byproduct of washing crushed gravel for concrete, and its unified classification is fine clayey sand (SC) with PI equals zero. Soil 2 is the clayey residue from washing sand obtained from rocks stored in sludge lakes, classified as low-compressibility clay (CL), with PI equals 35 %. Soil 3 consists of clayey residue from deep foundation excavations, classified as high-compressibility clay (CH) with PI equals 66 %. Table 4 presents the characterization results for each soil.

As shown in Fig. 5 and Table 4, the clayey residues have different compositions and characteristics. Fig. 5(a) Residue 1, SC, is a fine quartz sand covered by kaolin-type clay. The image shows the separation between grains, the formation of quartz and the kaolinite clay covering. Fig. 5(b) Residue 2, CL, consists of kaolinite clay. The formation of kaolinite sheets with porosities caused by swelling and dehydration is seen. Fig. 5(c) Residue 3, CH, is kaolinite clay with a high organic matter content, with the SEM image showing diatom remains typical of lake deposits.

2.2. Cement soil mix

Twenty-seven samples were prepared using the dosages listed in Table 5. The mix design was conducted following the compressive

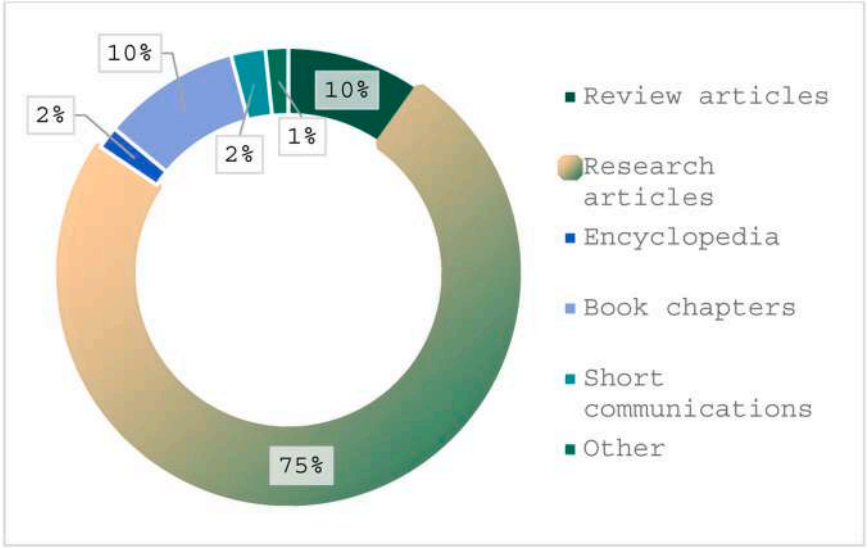

Fig. 2. Articles published since 2016, classified according to document type taken from the database ScienceDirect.

Table 1
Resilient Modulus (RM) of subgrades, calculation method and amount of data.

Source	Calculation Method	Year	Data	RM $_{min}$ (MPa)	RM $_{max}$ (MPa)	RM $_{mean.}$ (MPa)
[5]	Regression	1994	5	21	83	45.8
[6]	Matrix suction dependent model	2011	91	140	360	240
[7]	Multivariate regression	2019	30	30	180	110
[8]	Artificial neural network	2019	318	24.1	62.2	40.55
[9]	Finite elements method (FEM)	2020	50	12	290	120
[10]	Artificial neural network	2021	190	60	422	178.8
[11]	Regression	2020	144	43.4	343.1	179.5
[12]	Power Uzan	2021	30	60	460	250
[13]	Artificial neural network	2021	2103	3	360	34.87
[14]	Multivariate regression	2022	14	62	316	170.64
[15]	Monte Carlo Regression	2022	26	37.0	269.4	98.3
[16]	Finite elements method (FEM)	2022	57	5.08	327.42	83.08
[17]	Machine learning methods	2022	2816	3	217	33.8084
[18]	Finite elements method	2023	120	77	340	200
[19]	Bulk Stress Model	2023	5	28.1	115.9	55.3
[20]	Multivariate regression	2023	2	115	175	145
[21]	Power model	2023	12	212	330	256
[22]	Artificial neural network	2023	196	67.6	384.9	215.4
[23]	Regression	2024	80	15	124	72.5
[24]	Multi expression programming	2024	2813	3	217	33.808
[25]	Bagging Boosting	2024	2813	3	217	33.808
[26]	Finite elements method (FEM)	2024	20	160	90	115
[27]	Multivariate regression	2024	54	80	380	220
[28]	Machine Learning Models	2024	16	90	280	152.661
[29]	Regression	2024	9	73.2	166.42	114.89
[30]	Artificial neural network	2024	24	47	132	75
[31]	Smart Rock sensing	2024	36	148	378	268
[32]	XG Boost	2024	891	6.4	179.44	54.82

strength procedure described in the Portland Cement Association (PCA) guide, *Cement-Stabilized Subgrade Soils* [62]. High early strength (ART) performance cement was used, which also meets the specifications for Portland Cement Type I.

2.3. Data description

The data for this study were obtained from laboratory tests conducted with the selected materials. The database includes 2024 resilient modulus test results as the response parameter, a categorical variable representing the soil type, and 11 intervening variables: dry density, moisture content, cement content, compressive strength, indirect tensile strength, deviatoric stress, chamber pressure, organic matter content, and plasticity index.

2.4. Resilient module

The experimental resilience modulus tests were conducted at the Materials Research Group of Eafit University in Medellín, Colombia, using a GCTS hydraulic system capable of performing saturated or partially saturated triaxial tests. A mold with a height of 100 mm and a diameter of 50 mm was used. The samples were mixed by kneading and compacted with a monotonic compressive load on both sides (top and bottom) [63]. The samples were stored for 7 days in curing cabinets at temperatures of 10°C, 28°C, and 40°C, respectively. The resilient modulus tests were performed according to the AASHTO T307 standard method [64]. Preconditioning of the samples by thixotropy involved applying 500 loading cycles, which were not included in the database.

Fig. 6(a) shows the sample extraction method. The compaction and extraction process improves the quality of the samples. Fig. 6(b) presents a sample without cracks or imperfections. Fig. 6(c) shows the specimen in the chamber of the triaxial apparatus, and Fig. 6(d) shows it in the unconfined compression press. In both pieces of equipment, the specimen meets the required geometry, surface finish, and homogeneity. To validate the reliability of the samples, the effects of porosity on the test results were reviewed, revealing that variations in porosity did not significantly affect the resilient modulus or compressive strength.

2.5. Data description

The R Studio ecosystem was used, including packages for simple network models such as 'Neuralnet' and for more complex models such as 'H2O' for deep learning [65]. Neural networks are a deep learning algorithm inspired by the structure and function of the human brain. They consist of interconnected neurons organized in layers. Each neuron receives input from other neurons and produces an output [66]. The activation function determines the shape of the neuron's response; in this case, the sigmoid (logistic) function was used. This function transforms values in the range (-∞, +∞) to values in the range (0,1).

$$sigmoid(x) = \frac{1}{1 + \exp(-x)}$$

The weights of the connections between neurons are the parameters that the network learns during training and represent their strength. Neuron training is accomplished through a process called backpropagation, where the algorithm adjusts the weights of the connections to minimize the error between the predicted output and the actual output.

The process is based on four stages:

1. Understanding the structure of neural networks
2. Training neural networks
3. Designing the architecture of the neural network
4. Performance evaluation

Unlike multivariate trend models, neural network models are non-parametric, meaning they do not assume any specific distribution for the response variable, and it is not necessary for the variable to follow a normal distribution. The best way to evaluate a model is by predicting a set of observations that were not included in the training and optimization process [67].

3. Results and discussion

3.1. Temperature monitoring

After the samples were prepared, thermal conductivity was measured, and the internal temperature of the samples was monitored using a K-type Datalogger. Data was recorded every 15 min until 128 readings (32 h) were completed. As shown in Fig. 6, the samples reached room temperature after the first 200 min.

After 200 min, the samples generally maintained a constant temperature until they were 7 days old. It is worth noting that in the 40°C environment, the samples absorbed heat, causing their internal temperature to rise by 3–5 degrees. Meanwhile, the samples cured at 10°C reached a minimum temperature of 7.5°C. The samples cured at 28°C recorded minimum temperatures of 27°C and maximum temperatures of

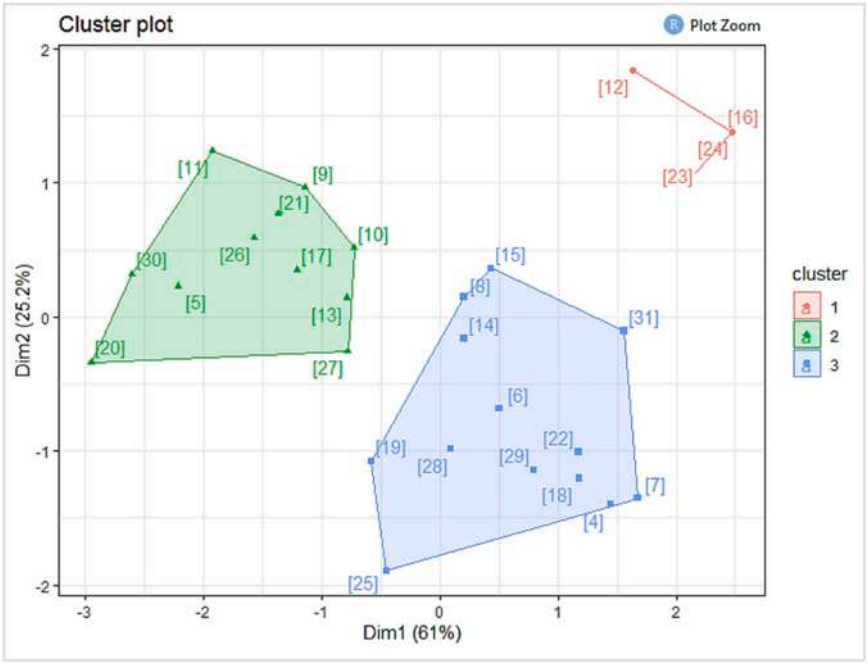

Fig. 3. Cluster plot using R Studio, by number source Table 1.

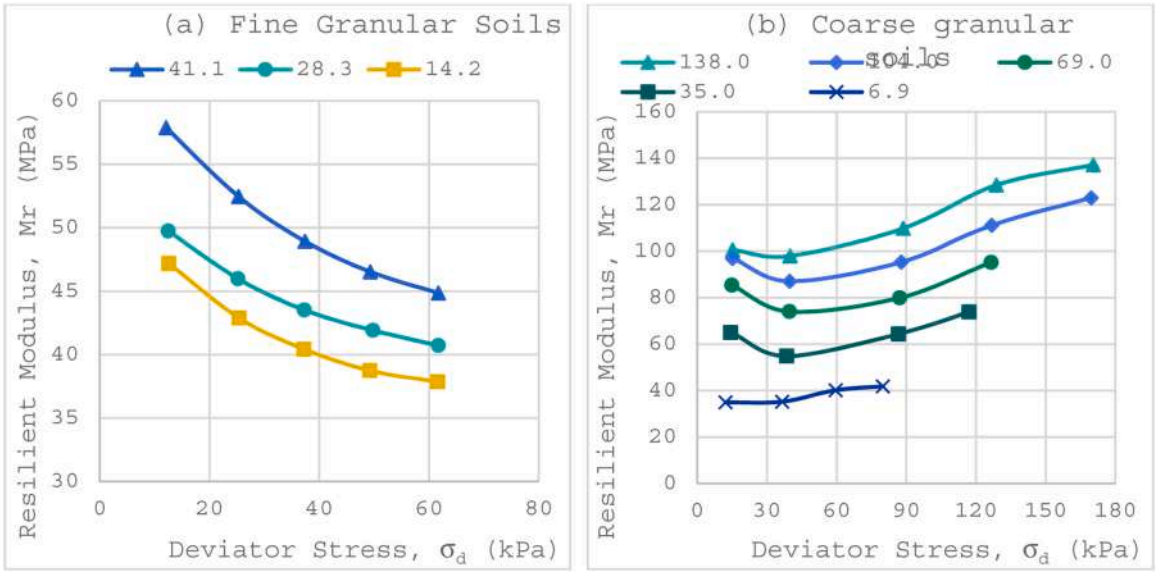

Fig. 4. Resilient modulus diagrams for fine and coarse granular soils, (a) Fine granular soils and (b) Coarse granular soils.

31°C.

By subtracting the minimum recorded temperature value from the average temperature during the first 32 h and dividing it by the constant ambient temperature, a percentage indicator of temperature or heat absorption is obtained. As shown in Fig. 8 the sandy clay sample absorbed more heat when cured at 40°C, but when cured at 10°C, it showed the least absorption. The CL and CH clay samples exhibited greater absorption when cured at 28°C and showed the same increase when cured at 10°C.(Fig. 7)

3.2. Descriptive statistics of data

According to the visual exploration of multicollinearity in Fig. 9, from the 2026 data points, a strong correlation (>0.90) can be identified between cement content and the loss on ignition or soil organic matter, the water content of the mixture, the plasticity index, and the dry unit weight.

The methylene blue index is inversely correlated with loss on ignition. Loss on ignition, or organic matter content, is inversely correlated with dry unit weight, indirect tensile strength, resilient modulus, and compressive strength. This means that the higher the organic matter content, the lower the mechanical strength.

The resilient modulus shows a significant relationship (>0.10) with all variables except thermal conductivity. The variables with the highest correlation to the resilient modulus (>0.9) are curing temperature, dry unit weight, methylene blue index, organic matter content, and compressive strength. Thermal conductivity is directly correlated with dry unit weight and the methylene blue index, and inversely correlated with curing temperature, plasticity index, water content of the mixture, and cement content.

Table 2
Studies of applying models in predicting Module Resilient.

M_R Model	Source
$Mr = K_1 * Pa * \left[\left(\frac{\sigma_3}{Pa}\right)^{K2}\right] * \left[\left(\frac{\sigma_d}{Pa} + 1\right)^{K3}\right]$	[41]
$Mr = K_1 * (Sm^{K2})$	[42]
$Mr = K_1 * (\sigma_d{}^{K2})$	[43]
$Mr = K_1 * (\sigma_d{}^{K2}) * (\sigma_3{}^{K3})$	[44]
$Mr = K_1 * Pa * \left[\left(\frac{(Bulk\ Stress - 3K6)}{Pa}\right)^{K2}\right] * \left[\left(\frac{Toct}{Pa} + K7\right)^{K3}\right]$	[45]
$M_R = K_1(\sigma_3)^{K_2}$	[46]
$\log Mr = C_1 + C_2 + W_c + C_3 \times S$	[47]
$Mr = K_1 * Pa * \left[\left(\frac{\sigma_3}{Pa}\right)^{K2}\right]$	[48]
$Mr = K_o\left(\frac{\sigma_1+\sigma_2+\sigma_3}{\frac{3}{Pa}}\right)^{K_1}\left(\frac{\tau_{oct}}{\tau_{ref}}\right)^{K_2}$	[49]
$Mr = K_1\left(\frac{\sigma_1\sigma_2+\sigma_2\sigma_3+\sigma_1\sigma_3}{\tau_{oct}}\right)^{K_2}$	[50]
$Mr = A_o + P_a + A_1 c + A_2 \times \sigma_d \tan\varnothing + A_3\theta + A_4 \times PaMC + A_5 UC$	[51]
$Mr = 10\left(a + \frac{b-a}{1+exp[\beta + K_2 \times (Wc - Wc_{opt})]}\right) \times K_1 Pa\left(\frac{\theta}{Pa}\right)^{K_2}\left(\frac{\tau_{oct}}{Pa}+1\right)^{K_3}$	[52]
$Mr = K_1 Pa\left[\left(\frac{\theta}{Pa}\right)^{K2}\right] * \left[\left(\frac{\tau_{oct}}{Pa} + 1\right)^{K3}\right]$	[53]
$Mr = K_1 Pa\left[\left(\frac{\sigma_b + 3K_4\varphi\theta}{Pa}\right)^{K_2}\right] * \left[\left(\frac{\tau_{oct}}{Pa} + 1\right)^{K3}\right]$	[54]
$Mr = K_1 Pa\left(\frac{\theta_b}{Pa}\right)^{K2}\left(K_4 + \frac{\tau_{oct}}{Pa}\right)^{K3} + \alpha_1 u_m{}^{\beta_1}$	[55]

Where: I: Thermal conductivity in W/mK, C_MPa: Compressive strength in MPa, T_MPa: Indirect tensile strength in MPa, Duw: Dry unit weight in Ton/m^3 , MBI: Methylene blue index, Tem: Curing temperature, IP: Plasticity index, W_S: Water content of the mix, LOI: Loss on ignition or organic matter content, C_S: Cement content in the mix, MR: Resilient Modulus in MPa, Cp: Cell pressure in kPa, Sd: Deviatoric stress in kPa and, n: Porosity of the sample.

The cement content (C_S) has an inverse relationship with mechanical strength (compression and tension). It is important to note that, for this experiment, each soil-cement mixture was prepared using the optimal cement dosage to achieve the same compressive strength. Therefore, the comparison of this variable should not be considered independently.

On the other hand, the box plot shown in Fig. 11 (a) indicates that the relationship between the resilient modulus and curing temperature is positive, meaning that a higher curing temperature corresponds to a higher resilient modulus. In Fig. 11 (b) The three types of soils used demonstrate that their physical and chemical characteristics, such as silica, kaolin, organic matter, and plasticity content, directly affect the resilient modulus. The CH material, characterized by the highest organic matter content, methylene blue index, and plasticity, records the lowest modulus values, while the SC sample, which is a non-plastic fine sand, records the highest modulus values.(Fig.10)

The Fig. 11 (c) shows how dry density increases depending on the soil type. It follows that higher silica content in soils increases density, while a higher plasticity index reduces the magnitude of dry density. These three variables influence the cement content of the mixture to some extent. Fig. 11 (d) illustrates that as the average cement content decreases, so does the resilient modulus. Finally, the chamber pressure observed in Fig. 11 (e) has an independent distribution in relation to the Mr results, similar to the dry density seen in Fig. 11 (f).

Checking the normality of the variable MR (Resilient Modulus),

Table 3
Schematic representation of a 3k design.

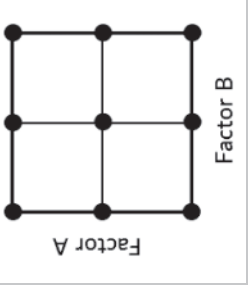

Curing Temperature	Soil	SC	CL	CH
10°C	3Mr	3Mr	3Mr	3Mr
28°C	3Mr	3Mr	3Mr	3Mr
40°C	3Mr	3Mr	3Mr	3Mr

Table 4
Physical and chemical characterization of Soil.

Soil	AASTHO	PI	Gs	I.A.M.	SiO_2	Al_2O_3	Fe_2O_3	CaO	MgO	LOI	Σ
SC	A−2–4	NP	2.33	3.40	80.1	8.9	4.4	0.18	2.42	4.0	100
CL	A−7–5	35 %	2.28	8.20	65.1	16.6	7.92	0.09	3.49	6.8	100
CH	A−7–6	66 %	1.76	10.00	62.0	16.7	3.7	0.7	3.2	13.7	100

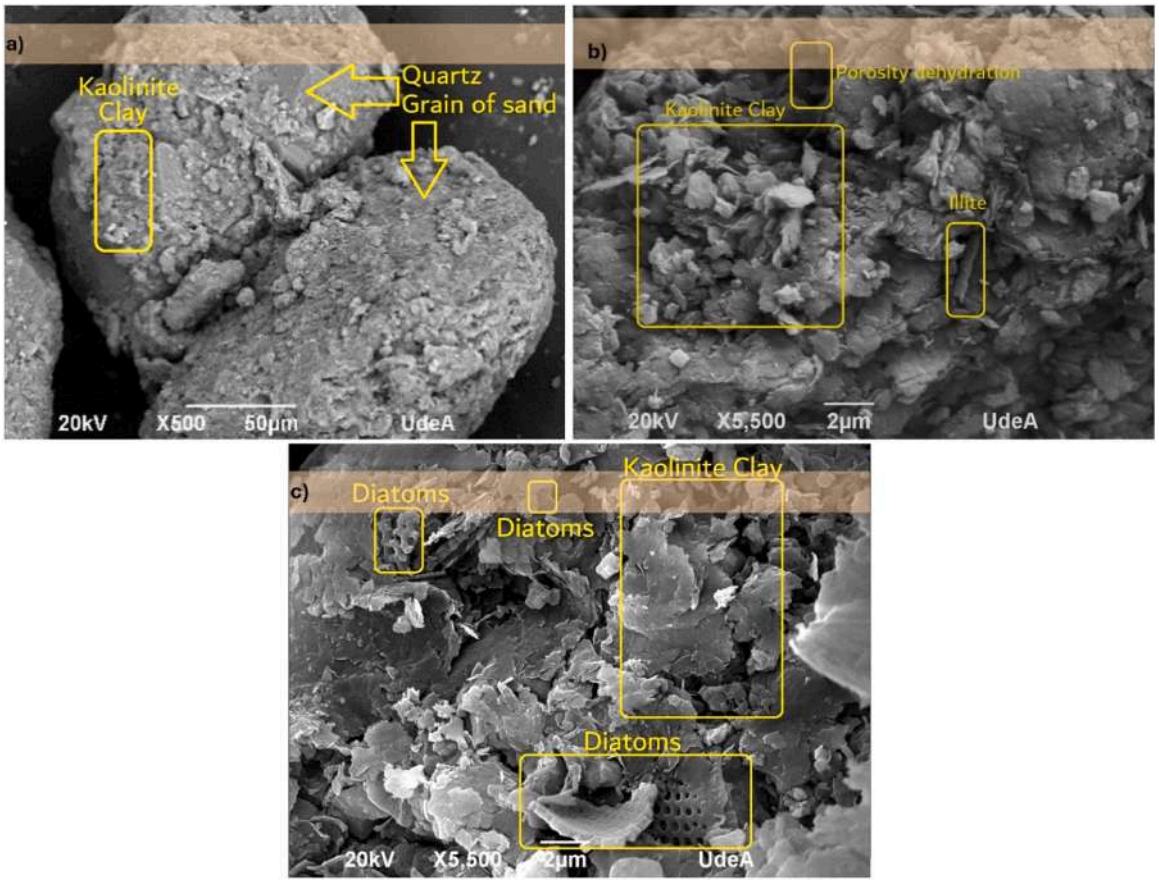

Fig. 5. SEM images of the clayey waste before mixing with hydraulic cement, a) Residue 1, b) Residue 2 and c) Residue 3.

Table 5
Mix design soil cement.

Soil	Cement/Soil Ratio	Water/Soil Ratio	Water/Cement Ratio
SC	0.125	0.170	1.36
CL	0.16	0.390	2.438
CH	0.42	0.616	1.467

Fig. 12 (a) shows a normal distribution with a mean of 154.28. The median is 143.85, the standard deviation is 54.13, and the coefficient of variation is 35 %. The coefficient of skewness is 0.57, indicating that the distribution is slightly skewed to the right. This suggests that some moduli may be higher than the mean. The kurtosis coefficient is 3.09, indicating a leptokurtic distribution. This suggests that the data is concentrated around the mean and exhibits relatively low variability.

Fig. 12 (b) shows the normality of the transformed variable with a leptokurtic distribution, while Fig. 12 (d) presents a normal distribution where only a few data points deviate toward the lower end, indicating that some results may be lower than the mean. Fig. 12 (c) demonstrates that the variable with the greatest effect on the resilient modulus is the curing temperature. Samples stored at 40°C exhibit the highest resilient moduli, whereas those stored at 10°C show the lowest modulus and the greatest variability.

The resilient modulus data expressed in linear models, which include the variables of chamber pressure, deviatoric stress, and temperature, are shown in Fig. 13. These models indicate that each type of soil, despite its physical and chemical differences, exhibits an increasing trend between deviatoric stress and temperature. The response surface that recorded the highest resistance corresponds to samples cured at 40°C, while the response surface that recorded the lowest modulus corresponds to samples cured at 10°C.

Fig. 13 (a) shows that the mixture with CH clay exhibits greater variability in the results. The highest Mr value approaches 350 MPa; however, under lower chamber pressures, this mixture achieves a lower average compared to the other two mixtures shown in Fig. 13 (b) and (c). The mixture with SC clearly registers the highest average modulus, displaying a steeper slope on the response surfaces in Fig. 13 (c). Indicating a positive effect of up to 18 % on the results of the resilient modules of samples cured at 40°C compared to those cured at temperatures of 28 and 10°C.

3.3. ANN model

After reviewing and cleaning the data using various statistical methods, an artificial neural network was created using two R Studio tools: Neuralnet and H2O.

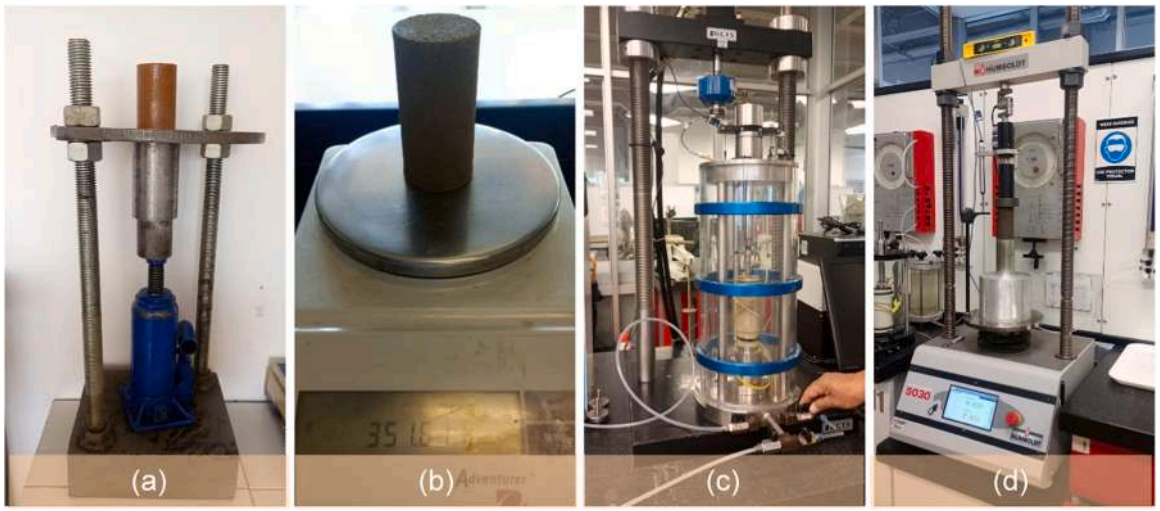

Fig. 6. Experimental process of the sample (a) molding, (b) measurement, (c) resilient modulus and (d) compression.

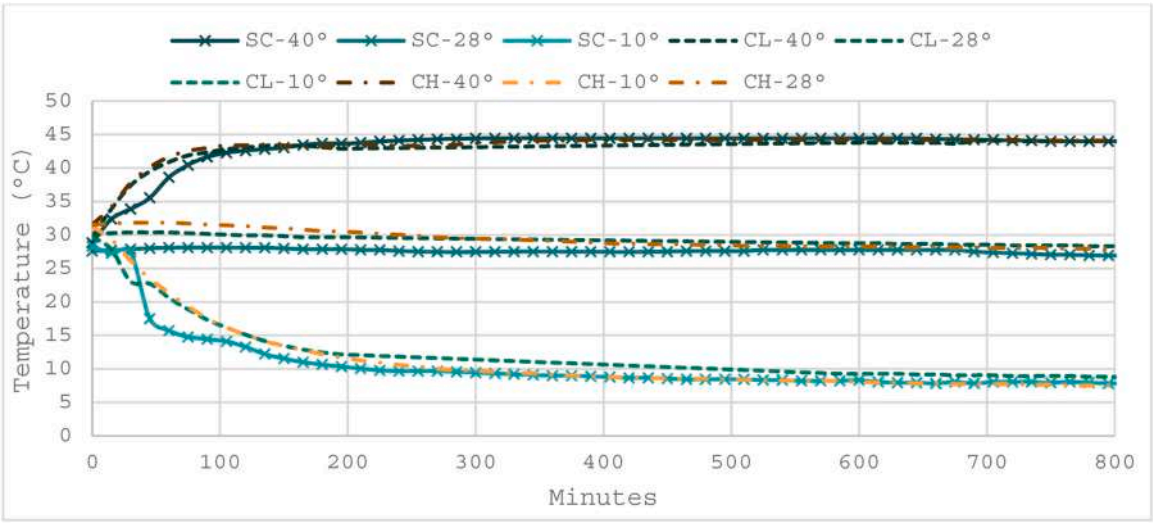

Fig. 7. Temperature variation during curing per minute (0–800).

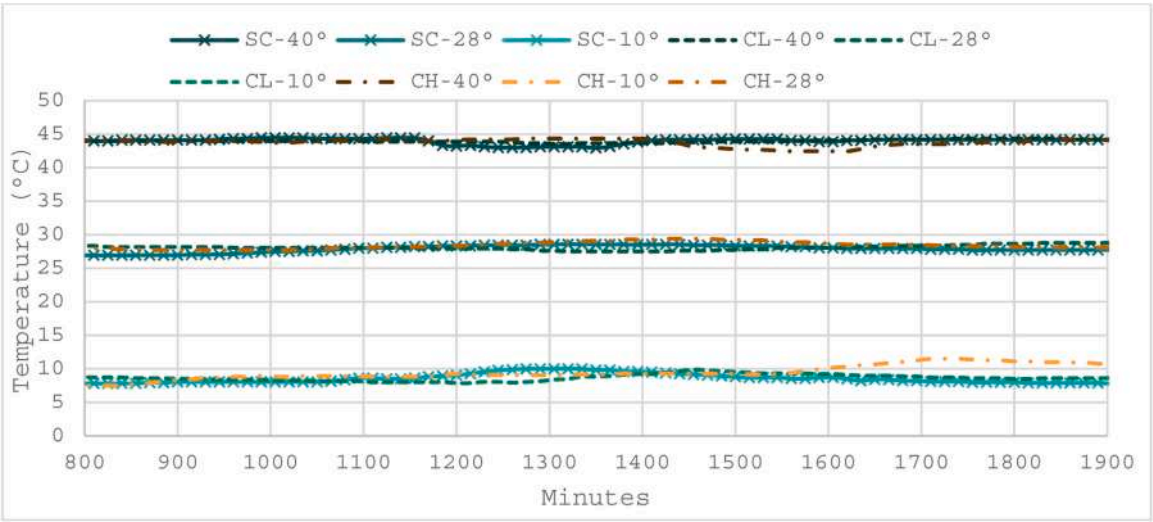

Fig. 8. Temperature variation during curing per minute (800–1900).

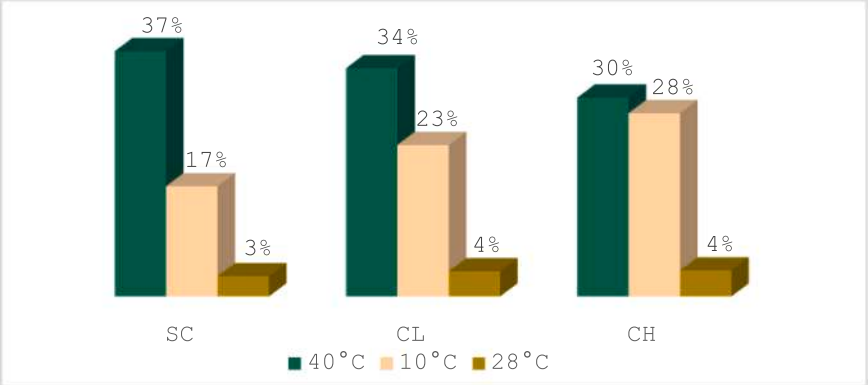

Fig. 9. % Heat absorption of the three types of mixtures cured at different temperatures.

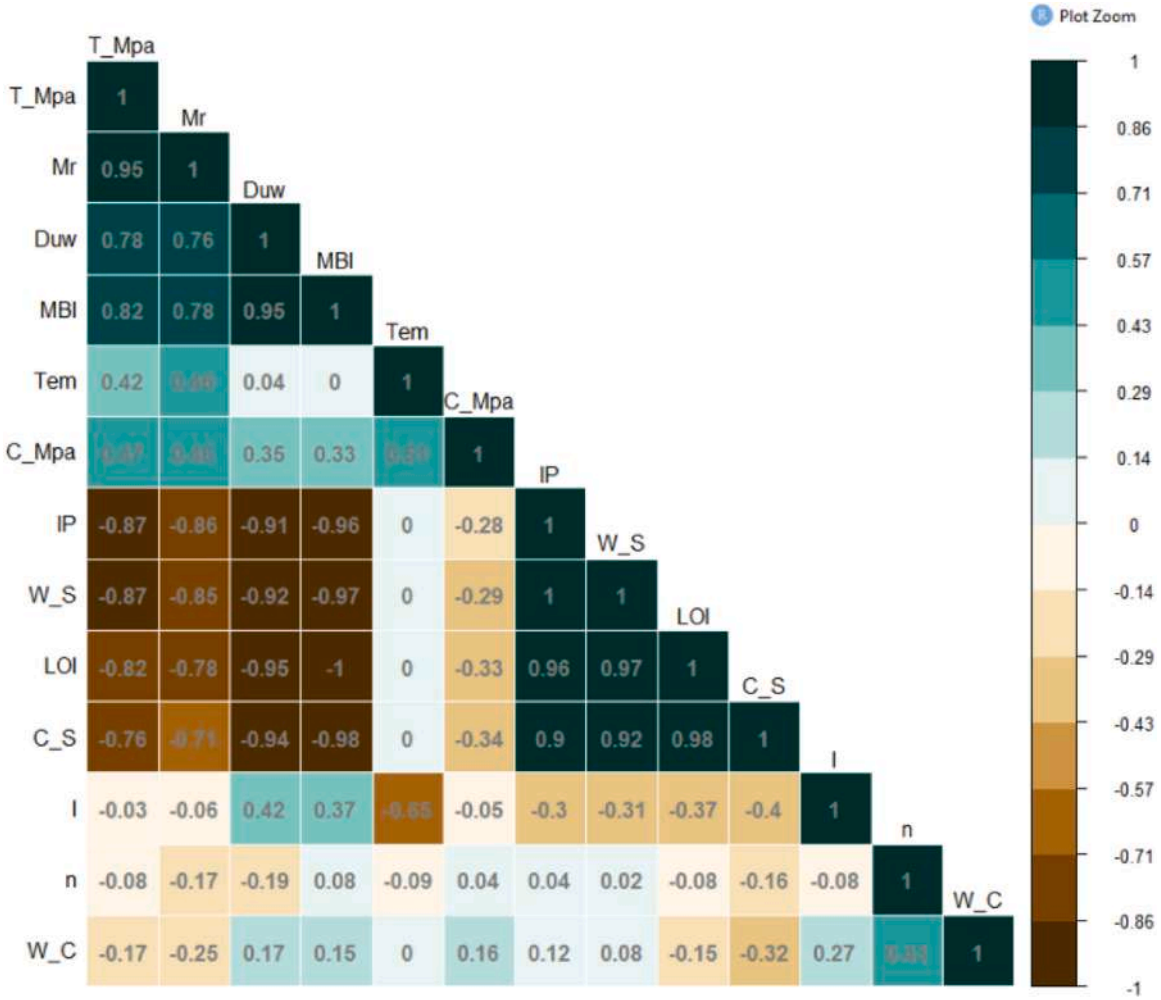

Fig. 10. Visual exploration on correlation matrix.

3.4. Neural network on neuralnet

This package is used for simple network models with straightforward architectures. The database has a distribution of variables that, when analyzed using the CA Biplot library, can help in selecting the variables involved in the model [68]. As shown in Fig. 14, the plot is asymmetric and displays a global pattern of the data. Rows are represented by blue points, and columns are represented by red text. The proximity between points reflects their similarity. It can be observed that compressive strength, density, and humidity are close to the water-cement ratio (W_C). Similarly, the indirect tensile strength (T_Mpa) is associated with the methylene blue index (MBI).

For this reason, the formula used for the ANN modeling is given as follows:

$C\_S \sim Tem + Mr + Sd + Cp + n + IP + LOI + MBI + C\_Mpa + T\_Mpa + Duw$, where C_S is the ratio between the cement content of the mixture, and the Mr is Resilient Module, Sd is the deviatoric stress in kPa, Cp is the cel pressure in kPa, n is the porosity of the sample, IP is the plasticity index, LOI

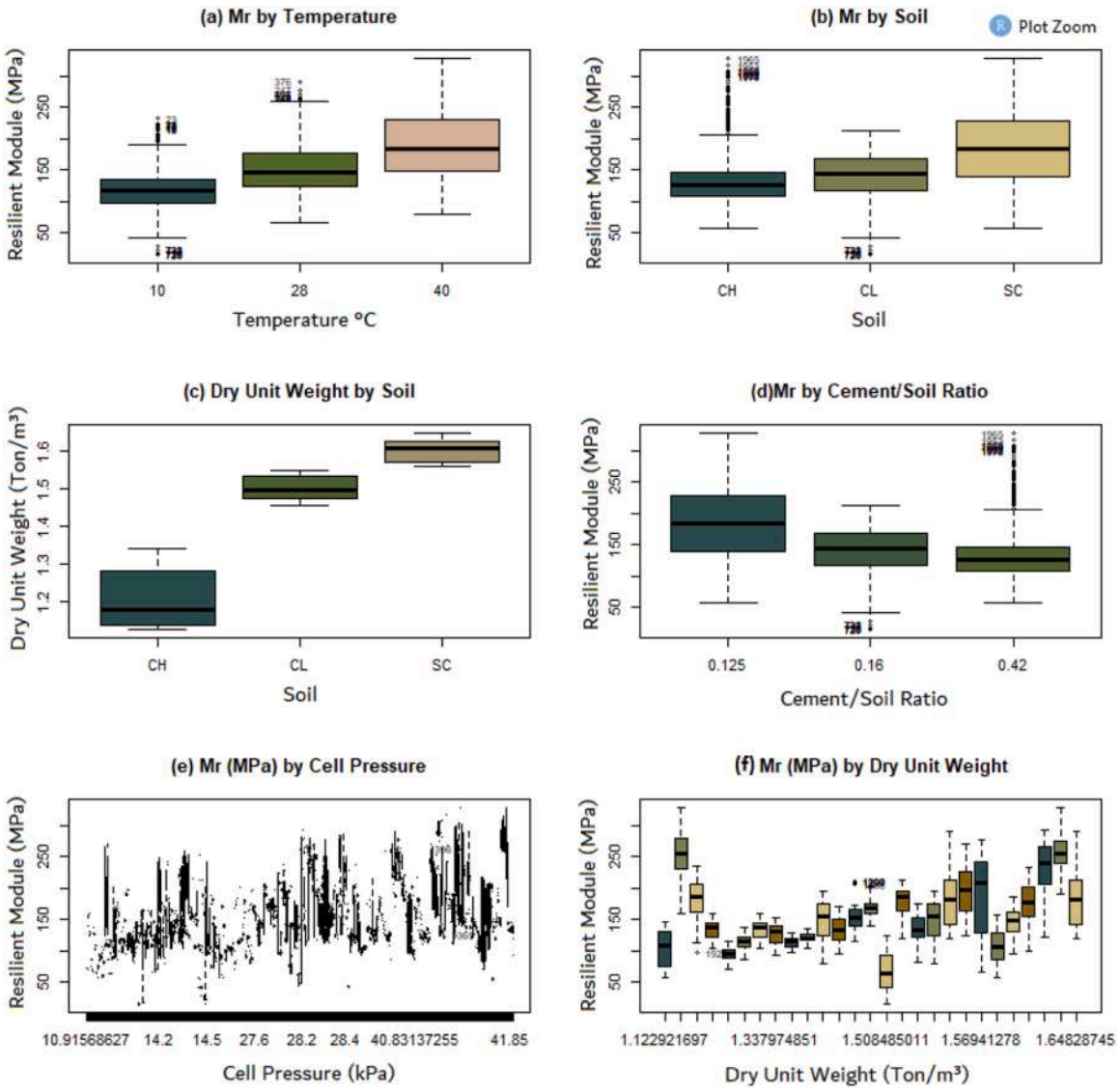

Fig. 11. Box plot of the intervening variables, (a) Resilient Module by Temperature, (b) Resilient Module by soil type, (c) Dry Unit Weight by soil type, (d) Resilient Module by Cement/Soil Ratio, (e) Resilient Module by Cell Pressure and (f) Resilient Module by Dry Unit Weight.

represents ignition losses or organic matter content, MBI is the methylene blue index, C_Mpa is de strength compression in MPa, T_Mpa is the indirect traction in MPa, and Duw is the dry unitary weigh.

The architecture with the lowest margin of error consists of 8 input neurons, two hidden layers—where the first hidden layer has 5 neurons and the second has 4 neurons. The activation function used was tanh, and the propagation algorithm executed was forward propagation with 'rprop+ .'

The techniques used to increase the efficiency of the neural network in this exercise can be summarized into four key steps. The first and most significant is that this research utilized its own dataset, developed with an experimental design that involved random, independent, and normalized data [69]. To achieve normalization, duplicate entries, redundancies, and noise were eliminated, and statistical techniques for the transformation and standardization of numerical data were applied. In this case, categorical data, such as soil type, were excluded, while numerical variables, such as the plasticity index, organic matter content, and methylene blue index, were included. The application of codes for modeling artificial neural networks requires all input variables to be rescaled to the same range, so the data were transformed using the 'scale' function.

The second technique is selecting the appropriate architecture. Different architectures were modeled, and the one that produced the smallest margin of error was selected.

The third technique involves advanced training methods, such as transfer learning, data augmentation, and batch training. In this case, only batch training was applied, as incorporating a larger dataset could have compromised the accuracy of the experiment [70]. However, the laboratory test used to estimate the resilient modulus is an efficient method for recording larger datasets, preventing the network from becoming overly specialized in the training data and struggling to model new examples.

The fourth technique refers to regularization methods to reduce weights and promote simplicity. In this case, since the architecture was simple, the modeling time was fast, and the results showed a low margin of error. As a result, no additional penalties were required, apart from those included in the code by default.

Fig. 15 (a) illustrates the architecture of the artificial neural network, where the thickness and color of the lines indicate the weights of each relationship between neurons. Thick black lines represent stronger positive weights, while thick gray lines indicate stronger negative weights. Fig. 15 (b) presents the numerical values of seven weights

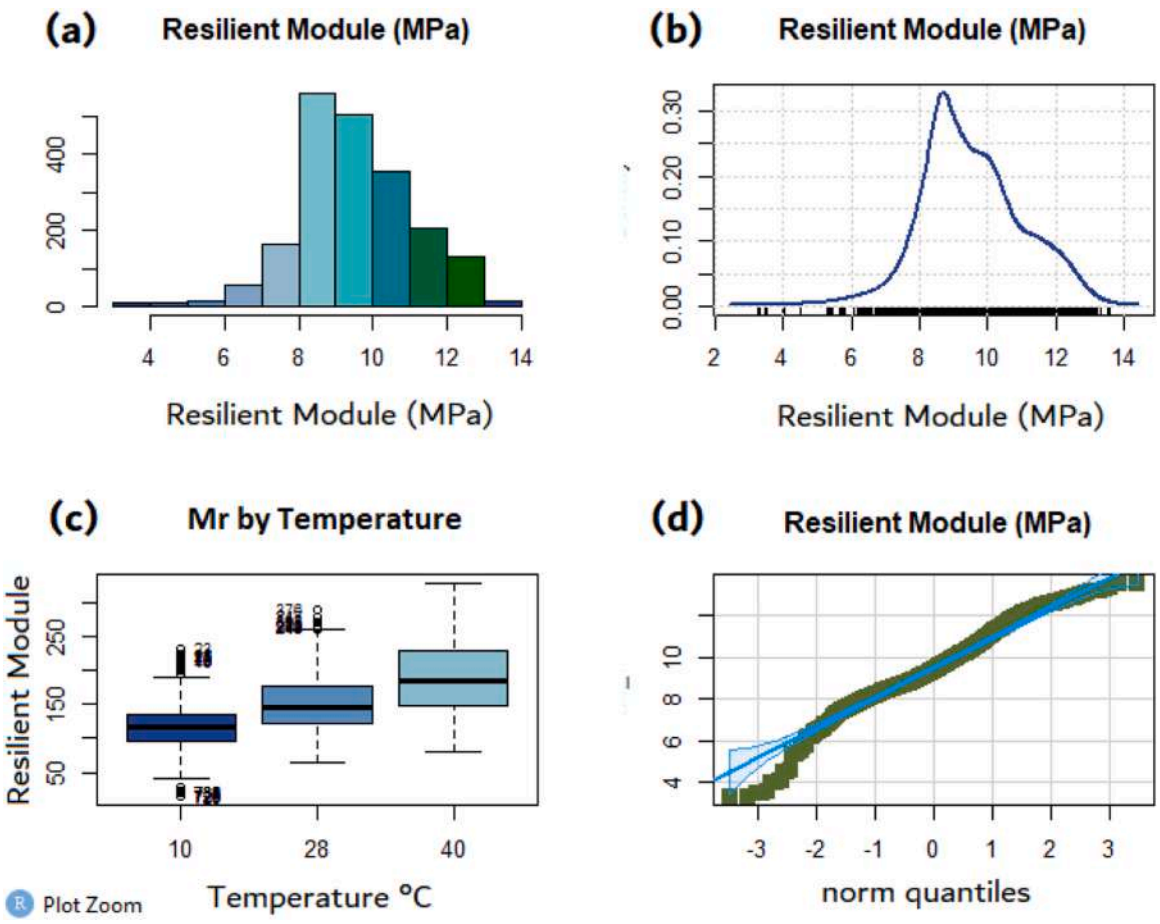

Fig. 12. Graphical description of the transformed variable Mr (Resilient Modulus in MPa), (a) Histogram Resilient Module (MPa), (b) Density Resilient Module (MPa), (c) Box plot Resilient Module by Temperature and (d) norm quantiles.

between each neuron.

On the other hand, the importance of the variables used in the model was identified in the training as shown in Fig. 16. The porosity of the mixture, the plasticity index, the organic matter content, and the curing temperature have an important effect on the calculation of the cement dosage.

3.5. ANN on H2O

Using the same data exploration procedures, transformations, predictor selection, and trend corrections, the database was loaded into the modeling using the Neuralnet package. In contrast, H2O has a greater capacity to handle millions of records on a single computer. Table 6 shows the numerical description of the variables that are part of the ANN model. To start training, it is necessary to exclude the categorical or character variables and perform the scaling of the numerical variables. (Table 7)

The importance of variables for neural network models is calculated using the Gedeon method. As shown in Fig. 17 (a), all variables have an importance level greater than 0.5, except for the deviatoric stress (Sd). Thermal conductivity (I) is the variable with the greatest effect on the neural network, followed by the methylene blue index, the simple compressive strength, and the curing temperature. These variables have a more direct impact on the cement content in a mixture than the resilient modulus. Fig. 17 (b) shows the accuracy of the training and model of the neural network, resulting in a very low RMSE, indicating high reliability in the model.

The H2O regression model, using deep learning, is set up with the following parameters: Neuron Layers status for predicting C_S, regression type, Gaussian distribution, quadratic loss, 162 weights/biases, 7.3 KB, and 16,170 training samples with a mini-batch size of 1.

As shown in the model recorded a lower margin of error with the following metrics: MSE (Mean Squared Error): 2.608923×10^{-5}, RMSE (Root Mean Squared Error): 0.005107762, MAE (Mean Absolute Error): 0.003892778, RMSLE (Root Mean Squared Logarithmic Error): 0.004372897, Mean Residual Deviance: 2.608923×10^{-5}, this represents high precision in the proposed model.

4. Conclusions

The objective of this study was to validate the resilience of mining and excavation waste under different curing temperatures. The aim was to design a tool to predict the optimal cement content required to transform this waste into cement-stabilized soil, achieving the necessary strength for pavement construction. A total of 81 samples were collected, generating 2026 resilient modulus data points under varying chamber pressures and deviatoric stresses. The characteristic variables of the mixtures were identified and statistically analyzed, and two R Studio codes were applied to predict the cement content with error margins below 0.001. The following key findings were identified:

- The temperature of the samples at time of mix start in 28–32 degrees Celsius. However, contrary to the typical exothermic reaction observed in hydraulic concretes, soil-cement mixtures absorb thermal energy from their environment through an endothermic process. This behavior can have positive effects on the use of mixtures in geothermal pavements. As cement-stabilized soil becomes a

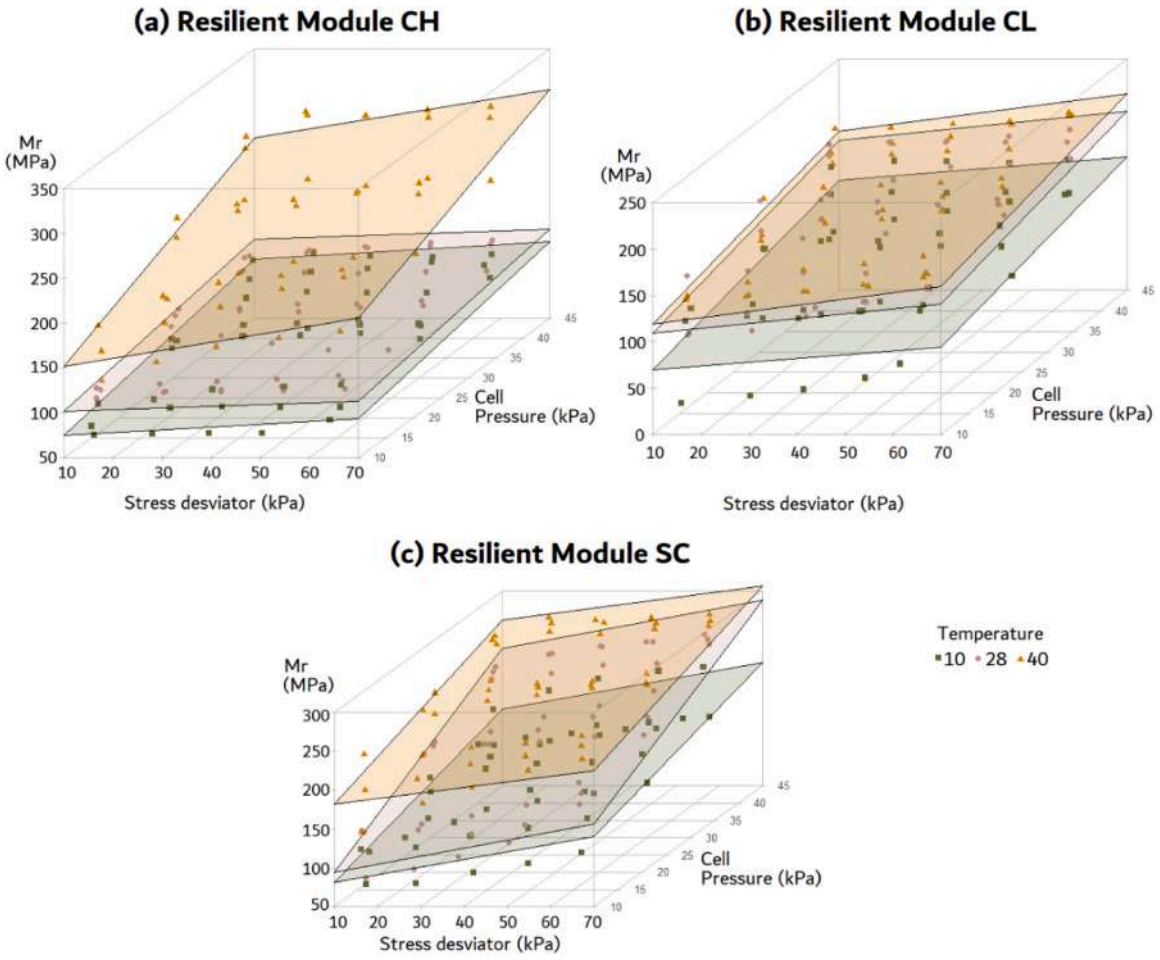

Fig. 13. Response surfaces of the resilient modules made to the three types of mixtures, (a) Samples Clay High Plasticity, (b) Samples Clay Low Plasticity and (c) Samples Sand Clayed.

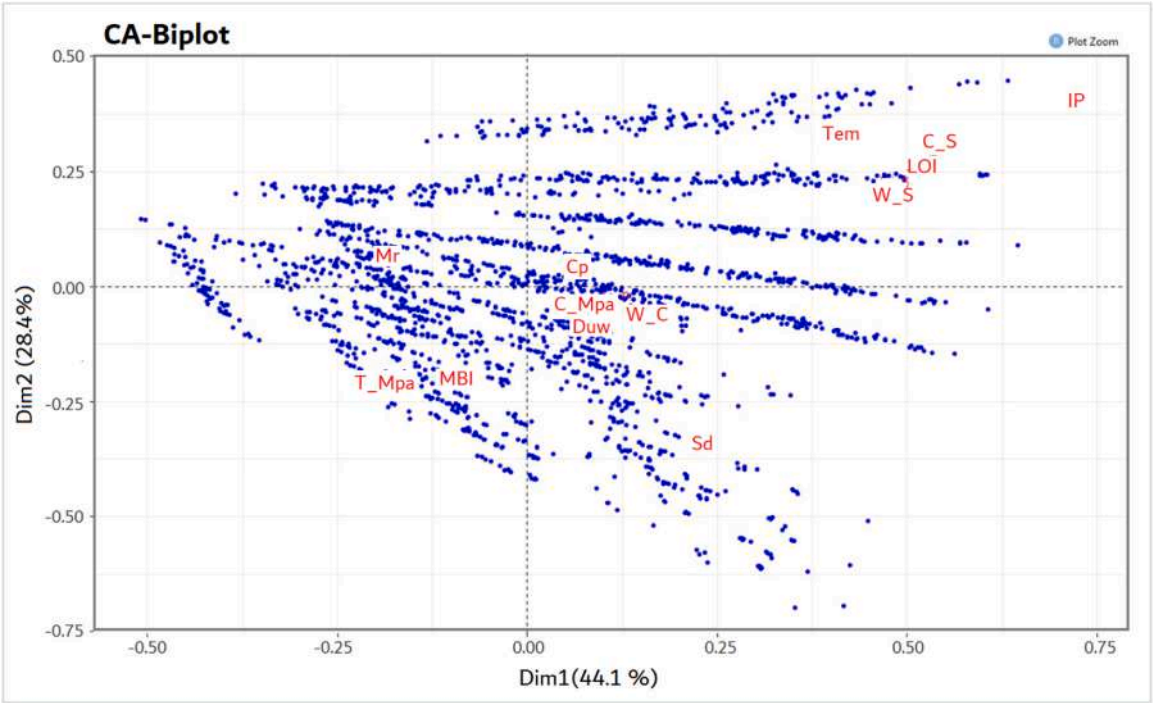

Fig. 14. Double column and row chart.

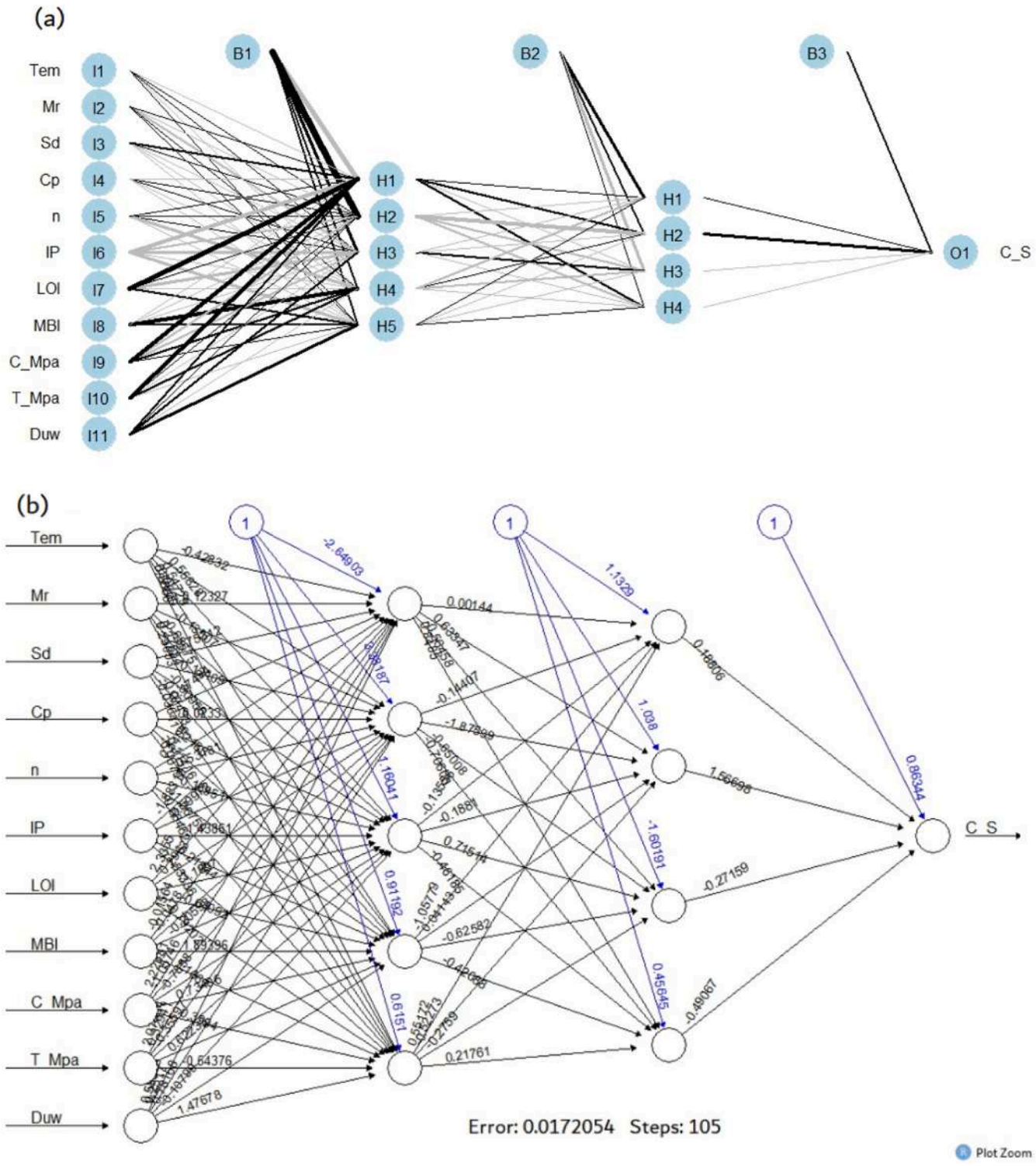

Fig. 15. Artificial Neural Network Architecture using Neuralnet, R Studio (a) model architecture and (b) model weights.

temperature-absorbing material, it can maintain and retaining heat for longer periods.

- It was identified that sandy materials, which have a high quartz content, have a greater capacity to absorb energy, resulting in significant temperature variations in environments with temperatures of 40°C. In contrast, clays absorb more energy at lower temperatures (10°C) and intermediate temperatures (28°C).
- It was identified that the thermal conductivity of the samples is directly proportional to the dry density and inversely proportional to the plasticity index, humidity, and ignition losses or organic matter content.
- The resilient modulus is directly proportional to the curing temperature, meaning that at higher temperatures, the resilient modulus measured at 7 days of curing is higher. Conversely, at lower temperatures, the resilient modulus is significantly lower. The effect of temperature must be considered when drafting standards and regulations for road construction. Since designs are based on laboratory tests conducted under controlled temperatures, replicating the

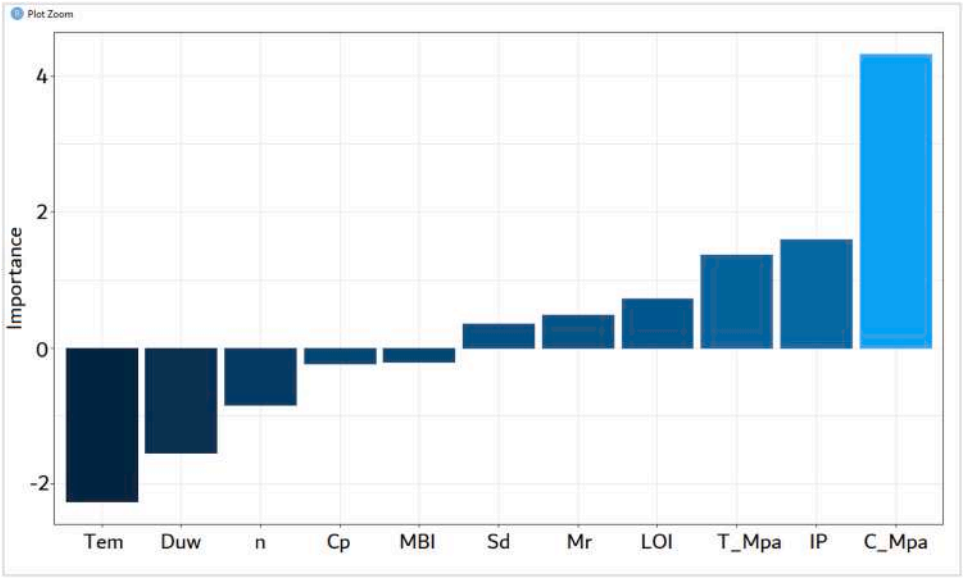

Fig. 16. Importance graph of input variables in the ANN, Neuralnet.

Table 6
Numerical description of the ANN model variables.

Code		Min.	Median	Mean	Max.
Soil	Soil	character	character	character	character
Tem	Temperature °C	10	28	26.01	40
Mr	Resilient Module (MPa)	13.98	143.85	154.29	328
Sd	Stress deviator (kPa)	9.991	36.958	37.313	67.19
Cp	Cell Pressure (kPa)	10.92	28.24	27.67	41.89
T_Mpa	Traction Stress (Mpa)	0.8553	2.6087	2.9941	5.874
C_Mpa	Compression Stress (Mpa)	2.434	2.865	2.957	3.788
Duw	Dry Unitary weight	1.123	1.497	1.436	1.648
n	Porosity	0.2361	0.3291	0.3227	0.3639
IP	Plasticity Index	0	0.35	0.3368	0.66
LOI	Loss on ignition	4	6.8	8.169	13.7
MBI	Methylene Blue Index	3.8	8.2	7.332	10
I	Thermal Conductivity	0.8953	1.4619	1.3764	1.6421
W_S	Water/Soil Ratio	0.17	0.39	0.3921	0.616
C_S	Cement/Soil Ratio	0.125	0.16	0.2351	0.42
W_C	Water/Cement Ratio	1.36	1.467	1.755	2.438

mixtures in different environmental conditions, particularly in cold climates, may not achieve the specified resilience outlined in the designs. For this reason, it should also be evaluated whether it is prudent to open roads to traffic at ages other than 7 days in areas with cold climates, where strength can be up to 18 % lower compared to those constructed in warm climates.

- In addition to curing temperature, variables that are related to resilient modulus are dry unit weight, compressive strength, chamber pressure and porosity. Unlike curing temperature, these variables can be controlled during the construction stage. For this reason, control measures must be implemented to ensure optimal compaction percentages. Regarding chamber pressure, it is a variable closely associated with the depth of the layer and its level of confinement. A confined pavement exhibits greater strength and durability compared to an unconfined pavement.
- Artificial neural network models not only facilitate the analysis involving many variables in the response but also provide useful predictions. The model created with Neuralnet recorded a margin of error of 0.0045. Although this error is not significant, it aids in developing the prediction model. On the other hand, the model using the H2O application was more efficient and faster, achieving an MSE of 0.000026.
- Modeling was performed using the response variable C_S (Cement content), as it is intended to be applied in mixture designs involving clayey waste with organic matter, cured at various temperatures. The values of resilient modulus and compressive strength serve as input data that can be utilized in pavement design.
- For a multivariate model to be efficient and statistically valid, the independence of the data, the normality of the data set, must be confirmed. In this case, H2O is more accurate than Neuralnet, however Neuralnet provides more information on weights between neurons and layers. This makes the analysis of the network easier for the designer, since it clearly identifies the neurons that can be replaced or eliminated from the model to make it cleaner and simpler.

Some of the limitations in applying this method include the requirement to account for all input variables during the experimental stage, such as compaction data, empty ratio, density, moisture, temperature, thermal conductivity, organic matter content, methylene blue index, among others. This forces the designer to determine all these inputs, which are of fixed size. The neural network architecture has a fixed number of input layers, meaning it can only accept one input and

Table 7
Model ANN, H2O R Studio.

layer	units	l1	l2	Mean rate	Rate rms	Mean weight	Weight rms	Mean bias	Bias rms
13	Input								
7	Rectifier	0	0	0.059211	0.033703	0.032746	0.294721	0.571969	0.095199
7	Rectifier	0	0	0.024918	0.017407	−0.04042	0.379233	1.014523	0.064902
1	Linear	0	0.00851	0.004233		0.05621	0.392236	−0.05428	0

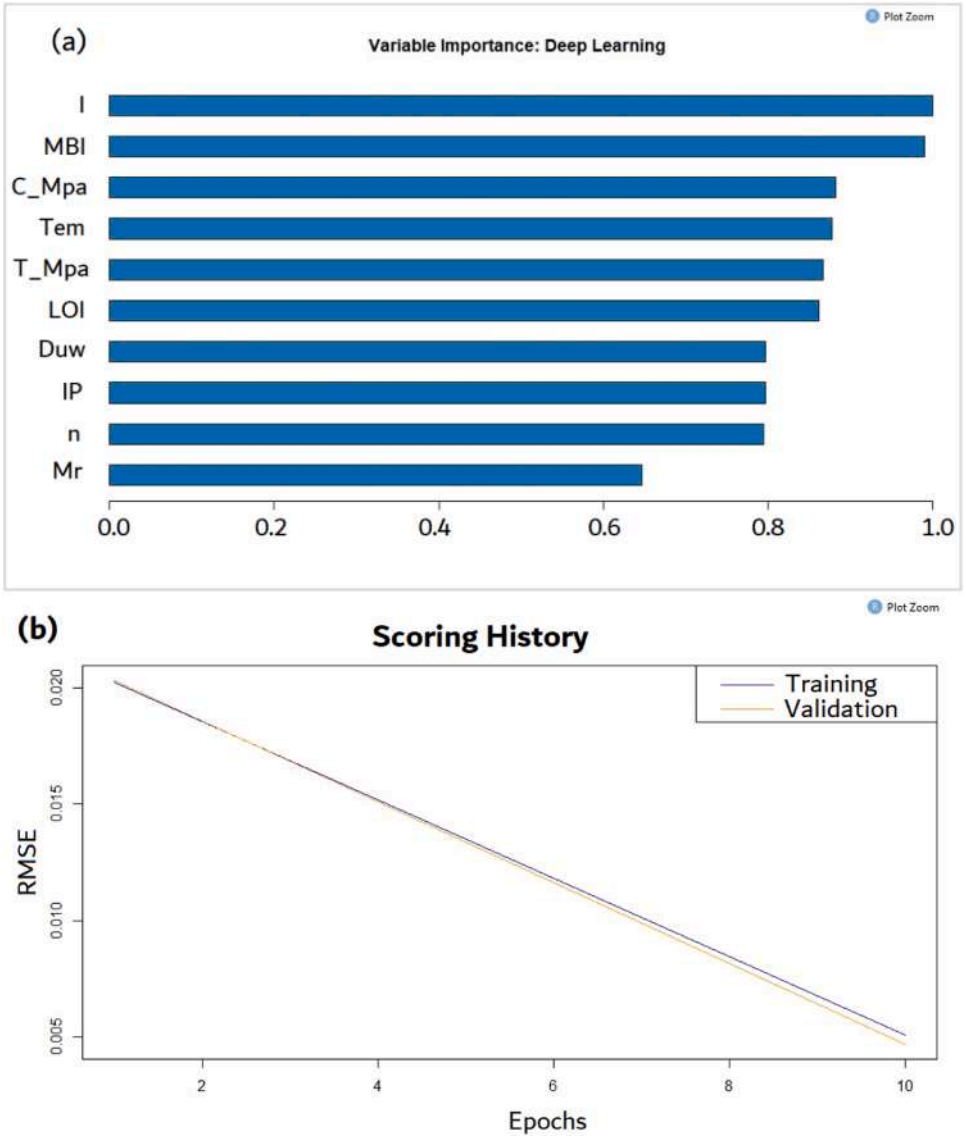

Fig. 17. (a) Variable Importance H2O, R Studio and (b) RMSE for Training and Validation of the ANN Model.

one output of fixed size for any given task. This becomes a limiting factor for many pattern recognition tasks.

Although the 3k experimental design is known to be suitable for non-linear models, the variability of the waste can affect the accuracy of the model. It is also important to note that this approach is applicable only to fine clayey waste and does not account for particle sizes larger than sieve No. 40 (0.425 mm).

Funding

This research did not receive financial support.

CRediT authorship contribution statement

Liliana Carolina Hernández García: Conceptualization, Methodology, Investigation, Writing – review & editing. **Julián Vidal Valencia**: Conceptualization, Methodology, Investigation, Supervision, Funding acquisition. **Henry A. Colorado L**: Conceptualization, Methodology, Investigation, Supervision, Funding acquisition.

Declaration of Competing Interest

The authors declare that they have no known competing financial interests or personal relationships that could have appeared to influence the work reported in this paper.

Acknowledgements

Liliana Hernandez would like to express our sincere gratitude to EAFIT University in Medellín for providing with the opportunity to undertake this enriching internship, especially like to thank Engineer Edgar Alexander Ossa, Wilmar Alonso Valles Bedoya, Wilfor Jesús Devia Pelaez and Bladimir de Jesús Rodríguez for these invaluable guidance and support throughout the entire process. Also, she acknowledges to Fondo Beca Doctoral Universidad de Antioquia for the fellowship for pursuing her PhD program.

Data availability

Data will be made available on request.

References

[1] United Nations (2023). The Sustainable Development Goals Report.
[2] E. Yaghoubi, B. Ghorbani, M. Saberian, R. van Staden, M. Guerrieri, S. Fragomeni, Strength and resilient modulus characteristics of emulsion-stabilized demolition wastes in pavement structures, J. Build. Eng. 82 (2024), https://doi.org/10.1016/j.jobe.2023.108257.
[3] L.C. Hernández García, S.N. Monteiro, H.A.C. Lopera, Recycling clay waste from excavation, demolition, and construction: trends and challenges, Sustainability 16 (2024), https://doi.org/10.3390/su16146265.
[4] A. Alnedawi, S. Ullah, A. Azam, E. Mousa, I. Obaid, A. Yosri, Integrated and holistic knowledge map of resilient modulus studies for pavement materials: a scientometric analysis and bibliometric review of research frontiers and prospects, Transp. Geotech. 33 (2022), https://doi.org/10.1016/j.trgeo.2021.100711.
[5] B. Dingqing Li, A. Member, E.T. Selig, Resilient modulus for fine-grained subgrade soils, J. Geotech. Eng. 120 (1994).
[6] C.E. Cary, C.E. Zapata, Resilient modulus for unsaturated unbound materials, Road. Mater. Pavement Des. 12 (2011) 615–638, https://doi.org/10.1080/14680629.2011.9695263.
[7] C. Gu, X. Ye, J. Wang, Y. Cai, Z. Cao, T. Zhang, Resilient behavior of coarse granular materials in three-dimensional stress state, Can. Geotech. J. 57 (2020), https://doi.org/10.1139/cgj-2019-0353.
[8] J. Ren, S.K. Vanapalli, Z. Han, K.O. Omenogor, Y. Bai, The resilient moduli of five Canadian soils under wetting and freeze-thaw conditions and their estimation by using an artificial neural network model, Cold Reg. Sci. Technol. 168 (2019), https://doi.org/10.1016/j.coldregions.2019.102894.
[9] J. Peng, J. Zhang, J. Li, Y. Yao, A. Zhang, Modeling humidity and stress-dependent subgrade soils in flexible pavements, Comput. Geotech. 120 (2020), https://doi.org/10.1016/j.compgeo.2019.103413.
[10] N. Heidarabadizadeh, A.R. Ghanizadeh, A. Behnood, Prediction of the resilient modulus of non-cohesive subgrade soils and unbound subbase materials using a hybrid support vector machine method and colliding bodies optimization algorithm, Constr. Build. Mater. 275 (2021), https://doi.org/10.1016/j.conbuildmat.2020.122140.
[11] L.C.H. García, N.F.L. Salamanca, Resilient module soil-cement prediction based on setting temperature, Ing. e Invest. 40 (2020) 7–13, https://doi.org/10.15446/ing.investig.v40n2.83120.
[12] M. Akbas, B. Ozaslan, R. Iyisan, Utilization of recycled concrete aggregates for developing high-performance and durable flexible pavements, Constr. Build. Mater. 407 (2023), https://doi.org/10.1016/j.conbuildmat.2023.133479.
[13] W. lie Zou, Z. Han, L. Ding, Qiang, Wang, X. Qun, Predicting resilient modulus of compacted subgrade soils under influences of freeze–thaw cycles and moisture using gene expression programming and artificial neural network approaches, Transp. Geotech. 28 (2021), https://doi.org/10.1016/j.trgeo.2021.100520.
[14] A. Yılmaz, Engineering properties of basalt aggregates in terms of use in granular layers of flexible pavements, Case Stud. Constr. Mater. 17 (2022), https://doi.org/10.1016/j.cscm.2022.e01182.
[15] S. Hanandeh, H. Ardah, A. Ardah, M. Abu-Farsakh, Prediction of the resilient modulus of stabilized weak subgrade for pavement design structure, Transp. Geotech. 37 (2022), https://doi.org/10.1016/j.trgeo.2022.100856.
[16] F. da Silva Martino Fonte, M. Donato, B.G. Gouveia, C.S.A. Santana, M.A. Vieira da Silva, Analysis of the influence of tropical soil classification methods on railway subgrades according to repeated load triaxial (RLT) and light weight deflectometer (LWD) tests, Case Stud. Constr. Mater. 17 (2022), https://doi.org/10.1016/j.cscm.2022.e01301.
[17] N. Kardani, M. Aminpour, M. Nouman Amjad Raja, G. Kumar, A. Bardhan, M. Nazem, Prediction of the resilient modulus of compacted subgrade soils using ensemble machine learning methods, Transp. Geotech. 36 (2022), https://doi.org/10.1016/j.trgeo.2022.100827.
[18] N. Avilés-Rojas, F. Suárez, A. Chamorro, A. González, Flood impact on structural response of asphalt pavement: a finite element modeling approach, Structures 57 (2023), https://doi.org/10.1016/j.istruc.2023.105259.
[19] Y. Bai, A. Arul rajah, S. Horpibulsuk, J. Chu, Gasified olive stone biochar as a green construction fill material, Constr. Build. Mater. 403 (2023), https://doi.org/10.1016/j.conbuildmat.2023.133003.
[20] K. Nasrollahi, J.C.O. Nielsen, E. Aggestam, J. Dijkstra, M. Ekh, Prediction of long-term differential track settlement in a transition zone using an iterative approach, Eng. Struct. 283 (2023), https://doi.org/10.1016/j.engstruct.2023.115830.
[21] M. Akbas, B. Özaslan, H. Khanbabazadeh, R. İyisan, Numerical study using stiffness parameters on the nonlinear behavior of RCA pavements under heavy traffic loads, Transp. Geotech. 29 (2021), https://doi.org/10.1016/j.trgeo.2021.100582.
[22] B. Indraratna, D.J. Armaghani, A. Gomes Correia, H. Hunt, T. Ngo, Prediction of resilient modulus of ballast under cyclic loading using machine learning techniques, Transp. Geotech. 38 (2023), https://doi.org/10.1016/j.trgeo.2022.100895.
[23] X. Cui, Y. Du, X. Zhang, J. Hao, Z. Bao, Q. Jin, X. Li, Characterizing the dynamic resilient modulus of subgrade soil treated by BT-SAP subjected to freeze-thaw cycles, Cold Reg. Sci. Technol. 220 (2024), https://doi.org/10.1016/j.coldregions.2024.104153.
[24] L. Khawaja, M.F. Javed, U. Asif, L. Alkhattabi, B. Ahmed, H. Alabduljabbar, Indirect estimation of resilient modulus (Mr) of subgrade soil: gene expression programming vs multi expression programming, Structures 66 (2024), https://doi.org/10.1016/j.istruc.2024.106837.
[25] L. Alkhattabi, K. Arif, Novel base predictive model of resilient modulus of compacted subgrade soils by using interpretable approaches with graphical user interface, Mater. Today Commun. 40 (2024), https://doi.org/10.1016/j.mtcomm.2024.109764.
[26] H. Fan, F. Gu, J. Zhang, J. Peng, J. Zheng, Back calculation of in-situ nonlinear viscoelastic properties of subgrade using a finite element-based machine learning approach, Transp. Geotech. 45 (2024), https://doi.org/10.1016/j.trgeo.2024.101205.
[27] M. Heidemann, D. Hasten Pflug, Experimental study on the resilient and permanent deformation of a compacted waste foundry sand, Transp. Geotech. 48 (2024), https://doi.org/10.1016/j.trgeo.2024.101319.
[28] A. Ramos, A. Gomes Correia, K. Nasrollahi, J.C.O. Nielsen, R. Calçada, Machine learning models for predicting permanent deformation in railway tracks, Transp. Geotech. 47 (2024), https://doi.org/10.1016/j.trgeo.2024.101289.
[29] M. Naeem, M.G. Arab, Y. Elbaz, M. Omar, H. Ezzat, W. Zeiada, Resilient behavior of bio-cemented sandy soil treated with enzyme-induced carbonate precipitation for pavement applications, Constr. Build. Mater. 411 (2024), https://doi.org/10.1016/j.conbuildmat.2023.134434.
[30] K. Riaz, N. Ahmad, Predicting resilient modulus: a data driven approach integrating physical and numerical techniques, Heliyon 10 (2024), https://doi.org/10.1016/j.heliyon.2024.e25339.
[31] S. Huang, Y. Qian, Correlating ballast resilient modulus with particle movement through smart rock sensing, Transp. Geotech. 47 (2024), https://doi.org/10.1016/j.trgeo.2024.101293.
[32] B. He, D.J. Armaghani, M.Z. Tsoukalas, C. Qi, R.M. Bhatawdekar, P.G. Asteris, A case study of resilient modulus prediction leveraging an explainable metaheuristic-based XG, Boost. Transp. Geotech. 45 (2024), https://doi.org/10.1016/j.trgeo.2024.101216.
[33] N. Akbarpour, E. Akbari, H. Motameni, External clustering validity index based on extended similarity measures, J. Comput. Sci. 72 (2023), https://doi.org/10.1016/j.jocs.2023.102116.
[34] S. Hanandeh, A. Ardah, M. Abu-Farsakh, Using artificial neural network and genetics algorithm to estimate the resilient modulus for stabilized subgrade and propose new empirical formula, Transp. Geotech. 24 (2020), https://doi.org/10.1016/j.trgeo.2020.100358.
[35] M.C. Cavalli, D. Chen, Q. Chen, Y. Chen, A. Cannone Falchetto, M. Fang, H. Gu, Z. Han, Z. He, J. Hu, et al., Review of advanced road materials, structures, equipment, and detection technologies, J. Road. Eng. 3 (2023) 370–468, https://doi.org/10.1016/j.jreng.2023.12.001.
[36] Seed, H.B., and Chan, C.K. (1961). Effect of Duration of Stress Application on Soil Deformation Under Repeated Loading. 5th International Conference on Soil Mechanics and Foundation Engineering (Paris), 341–345.
[37] Brizuela, L.G., Alderete, N.M., and Rivera, J.J. "Procedimiento de moldeo para suelos granulares complementario a la Norma AASTHO T-307 para el ensayo de Módulo Resiliente de suelos viales."
[38] L.C. Hernández García, H.A. Colorado Lopera, Effect of the loss on ignition on the unconfined compressive strength of residual clays from Bogotá-Colombia stabilized with cement, J. Mater. Res. Technol. 33 (2024) 7123–7135, https://doi.org/10.1016/j.jmrt.2024.11.081.
[39] B. Dingqing Li, E.T. Selig, Resilient modulus for fine-grained subgrade soils, J. Geotech. Eng. 120 (1994) 939–957.
[40] Hicks, R.G., and Monismith, C.L. (1971). Factors influencing the Resilient Response of Granular Materials.
[41] M.W. Witczak, J. Uzan, The universal airport pavement design system, Report I of IV: Granular material characterization, University of Maryland, College Park, MD, 1988.
[42] R. Pezo, W.R. Hudson, Prediction models of resilient modulus for nongranular materials, Geotech. Test. J. 17 (1994) 349–355, https://doi.org/10.1520/GTJ10109J.
[43] Kim, D.-G. (2004). DEVELOPMENT OF A CONSTITUTIVE MODEL FOR RESILIENT MODULUS OF COHESIVE SOILS.
[44] Highway Research Board (1967). Prediction of flexible pavement deflections from laboratory repeated-load test (California).
[45] M.S. Jin, K.W. Lee, W.D. Kovacs, Seasonal variation of resilient modulus of subgrade soils, J. Transp. Eng. 120 (1994) 603–616, https://doi.org/10.1061/(ASCE)0733-947X(1994)120:4(603).
[46] J. Moossazadeh, M.W. Witczak, Prediction of subgrade moduli for soil that exhibits nonlinear behavior, Transp. Res. Rec. (1981) 9–17.
[47] R.W. May, M.W. Witczak, Effective granular modulus to model pavement responses, Transp. Res. Rep. (1981) 1–9.
[48] T.C. Johnson, R.L. Berg, A. DiMillio, Frost action predictive techniques: an overview of research results, Transp. Res. Rec. (1986).
[49] P. Tian, M.M. Zaman, J.G. Laguros, Gradation and moisture effects on resilient moduli of aggregate bases, Transp. Res. Rec. (1986).
[50] Dragos, A. (2003). Development of a predictive model for the Resilient Modulus of Unbound materials.
[51] NCHRP (2004). Laboratory Determination of Resilient Modulus for Flexible Pavement Design (2004). Transportation Research Record, 1–48. 10.17226/21960.
[52] J.H. Oh, E.G. Fernando, C. Holzschuher, D. Horhota, Comparison of resilient modulus values for Florida flexible mechanistic-empirical pavement design, Int. J. Pavement Eng. 13 (2012) 472–484, https://doi.org/10.1080/10298436.2011.633170.
[53] Z. Han, S.K. Vanapalli, State-of-the-art: prediction of resilient modulus of unsaturated subgrade soils, Int. J. Geomech. 16 (2016), https://doi.org/10.1061/(ASCE)gm.1943-5622.0000631.
[54] B. Ghorbani, A. Arulrajah, G. Narsilio, S. Horpibulsuk, M. Leong, Resilient moduli of demolition wastes in geothermal pavements: experimental testing and ANFIS

modelling, Transp. Geotech. 29 (2021), https://doi.org/10.1016/j.trgeo.2021.100592.
[55] Y. Motamedi, N. Makasis, S. Düber, G.A. Narsilio, A. Arulrajah, S. Horpibulsuk, Field investigation on geothermal pavements, Geomech. Energy Environ. 35 (2023), https://doi.org/10.1016/j.gete.2023.100475.
[56] M. Cetin, M. Ozenen Kavlak, M.A. Senyel Kurkcuoglu, G. Bilge Ozturk, S.N. Cabuk, A. Cabuk, Determination of land surface temperature and urban heat island effects with remote sensing capabilities: the case of Kayseri, Türkiye, Nat. Hazards 120 (2024) 5509–5536, https://doi.org/10.1007/s11069-024-06431-5.
[57] Y. Motamedi, N. Makasis, X. Gu, G.A. Narsilio, A. Arulrajah, S. Horpibulsuk, Investigating the thermal behaviour of geothermal pavements using thermal response test (TRT), Transp. Geotech. 29 (2021) 100576, https://doi.org/10.1016/j.trgeo.2021.100576.
[58] A. Mahpour, T. El-Diraby, Incorporating climate change in pavement maintenance policies: application to temperature rise in the Isfahan County, Iran, Sustain Cities Soc. 71 (2021), https://doi.org/10.1016/j.scs.2021.102960.
[59] L.A. Balan, B.R. Anupam, S. Sharma, Thermal and mechanical performance of cool concrete pavements containing waste glass, Constr. Build. Mater. 290 (2021), https://doi.org/10.1016/j.conbuildmat.2021.123238.
[60] K. Kim, S. Chun, B. Park, S. Han, Precast prestressed concrete pavement (PPCP): Effect of thermal gradient on curling deflection and stress, Constr. Build. Mater. 274 (2021), https://doi.org/10.1016/j.conbuildmat.2020.121966.
[61] Jerod, G., and Wayne, A. (2020). Cement-Stabilized Subgrade Soils.
[62] G. Hernández, L.C, N.F. Lizarazo, Resilient module soil-cement prediction based on setting temperature, Ing. e Investig. 40 (2020) 1–7, https://doi.org/10.15446/ing.investig.v40n2.83120.
[63] AASHTO, A.A. of S.H. and T.O (2020). Mechanistic Empirical Pavement Design Guide (Washington: AASHTO MEPDG-3).
[64] J. Amat Rodrigo, Machine Learning con H2O y R, Cienc. De. Datos (2020) 1–58.
[65] V.R. Konasani, S. Kadre, Machine Learning and Deep Learning Using Python and TensorFlow, McGraw Hill, 2021.
[66] Najmi, A.-H., and Todd K., M. (2020). Advanced Signal Processing: A Concise Guide. Neural Networks, Chapter (New York).
[67] Y. Zhao, K. Zhang, F. Dong, Y. Luo, S. Liu, Automated gradation design of natural waste gravel soil stabilized by composite soil stabilizer based on a novel DNNSS-APDM-PFC model, Waste Manag. 194 (2025) 64–76, https://doi.org/10.1016/j.wasman.2024.12.046.
[68] X. Li, Z. Chen, L. Huang, B. Li, J. Yan, P. Zhang, Z. Liu, Life cycle dynamic formation temperature response and thermal energy extraction of mine geothermal system considering groundwater flow, Int. J. Min. Sci. Technol. (2025), https://doi.org/10.1016/j.ijmst.2024.12.011.
[69] R. Li, S. Wang, J. Ma, W. Liu, T. Wu, C. Xie, X. Wu, Y. Ding, L. Zhao, G. Hu, et al., The impacts of soil enthalpy change on land–atmosphere interactions of permafrost on the Qinghai-Tibet Plateau, Geoderma 454 (2025) 117183, https://doi.org/10.1016/j.geoderma.2025.117183.
[70] A.T. Al-Sayegh, N.S. Mahmoudabadi, F. Shabbir, F.J. Alkandari, S. Saghir, A. Ahmad, Prediction of load-bearing capacity of RC columns (CWA) using artificial neural networks (ANN) trained on a hybrid experimental database HEXP, J. Eng. Res. (Kuwait) (2025), https://doi.org/10.1016/j.jer.2024.12.014.